Early Results from GLASS-JWST. XIII. A Faint, Distant, and Cold Brown Dwarf [*]

Mario Nonino[1], Karl Glazebrook[2], Adam J. Burgasser[3], Gianluca Polenta[4], Takahiro Morishita[5], Marius Lepinzan[1], Marco Castellano[6], Adriano Fontana[6], Emiliano Merlin[6], Andrea Bonchi[4], Diego Paris[6], Tommaso Treu[7], Benedetta Vulcani[8], Xin Wang[9], Paola Santini[6], Eros Vanzella[10], Themiya Nanayakkara[2], Amata Mercurio[11], Piero Rosati[12], Claudio Grillo[13,14], and Marusa Bradac[15,16]

[1] INAF-Trieste Astronomical Observatory, Via Bazzoni 2, I-34124, Trieste, Italy; mario.nonino@inaf.it
[2] Centre for Astrophysics and Supercomputing, Swinburne University of Technology, PO Box 218, Hawthorn, VIC 3122, Australia
[3] Department of Physics, University of California San Diego, La Jolla, CA 92093, USA
[4] Space Science Data Center, Italian Space Agency, via del Politecnico, I-00133, Roma, Italy
[5] IPAC, California Institute of Technology, MC 314-6, 1200 E. California Boulevard, Pasadena, CA 91125, USA
[6] INAF Osservatorio Astronomico di Roma, Via Frascati 33, I-00078 Monteporzio Catone, Rome, Italy
[7] Department of Physics and Astronomy, University of California, Los Angeles, 430 Portola Plaza, Los Angeles, CA 90095, USA
[8] INAF Osservatorio Astronomico di Padova, vicolo dell'Osservatorio 5, I-35122 Padova, Italy
[9] Infrared Processing and Analysis Center, Caltech, 1200 E. California Boulevard, Pasadena, CA 91125, USA
[10] INAF—OAS, Osservatorio di Astrofisica e Scienza dello Spazio di Bologna, via Gobetti 93/3, I-40129 Bologna, Italy
[11] INAF—Osservatorio Astronomico di Capodimonte, Via Moiariello 16, I-80131 Napoli, Italy
[12] Dipartimento di Fisica e Scienze della Terra, Università degli Studi di Ferrara, Via Saragat 1, I-44122 Ferrara, Italy
[13] Dipartimento di Fisica, Universitá degli Studi di Milano, Via Celoria 16, I-20133 Milano, Italy
[14] INAF—IASF Milano, via A. Corti 12, I-20133 Milano, Italy
[15] University of Ljubljana, Department of Mathematics and Physics, Jadranska ulica 19, SI-1000 Ljubljana, Slovenia
[16] Department of Physics and Astronomy, University of California Davis, 1 Shields Avenue, Davis, CA 95616, USA

Abstract

We present the serendipitous discovery of a late T-type brown dwarf candidate in JWST NIRCam observations of the Early Release Science Abell 2744 parallel field. The discovery was enabled by the sensitivity of JWST at 4 μm wavelengths and the panchromatic 0.9–4.5 μm coverage of the spectral energy distribution. The unresolved point source has magnitudes F115W = 27.95 ± 0.15 and F444W = 25.84 ± 0.01 (AB), and its F115W−F444W and F356W−F444W colors match those expected for other known T dwarfs. We can exclude it as a reddened background star, high redshift quasar, or a very high redshift galaxy. Comparison with stellar atmospheric models indicates a temperature of $T_{\rm eff} \approx 650$ K and surface gravity log $g \approx 5.25$, implying a mass of 0.03 $M_\odot$ and age of 5 Gyr. We estimate the distance of this candidate to be 570–720 pc in a direction perpendicular to the Galactic plane, making it a likely thick disk or halo brown dwarf. These observations underscore the power of JWST to probe the very low-mass end of the substellar mass function in the Galactic thick disk and halo.

Unified Astronomy Thesaurus concepts: T dwarfs (1679)

1. Introduction

A significant fraction of Milky Way stars near the Sun are cool brown dwarfs, nonfusing stars that have masses $M \leqslant 0.07\,M_\odot$, effective temperatures (in the field) of $T_{\rm eff} \leqslant 2000$ K, and are classified as late-*L, T,* and *Y* dwarfs (Kumar 1962; Chabrier & Baraffe 2000; Kirkpatrick 2005). These objects are intrinsically faint and emit primarily at infrared wavelengths. Hence, wide-field imaging surveys of brown dwarfs are largely limited to the immediate solar neighborhood ($d \leqslant 100$ pc), and few metal-poor thick disk and halo brown dwarfs have been identified to date (Burgasser et al. 2003; Zhang et al. 2019; Schneider et al. 2020). Deep pencil-beam surveys, conducted primarily with the Hubble Space Telescope (HST) WFC3 instrument, have extended brown dwarf detection to J ≈ 25.5 (AB), reaching kiloparsec scales (Ryan et al. 2011; Masters et al. 2012; Aganze et al. 2022). However, these surveys are restricted to wavelengths < 2 μm,

limiting their sensitivity to the reddest and coldest brown dwarfs. The JWST represents a major step forward in the detection of cool and distant brown dwarfs, with imaging and spectroscopy extending to ∼28.3 μm and providing orders of magnitude greater sensitivity than Spitzer, particularly in the 3–5 μm wavelength range where cold brown dwarf spectral energy distributions peak.

The availability of the deep JWST NIRCam observations in a deep extragalactic field have provided the first opportunity to study low-temperature brown dwarfs in the Galactic thick disk and halo. In this paper, we report the first detection of such an object. In Section 2, we summarize the JWST observations. In Section 3, we present the identification of the brown dwarf candidate, and compare its colors and magnitudes to theoretical models to estimate its physical properties. We also rule out potential contaminant sources. In Section 4, we present our conclusions. In this paper, we use the AB magnitude system unless otherwise indicated.
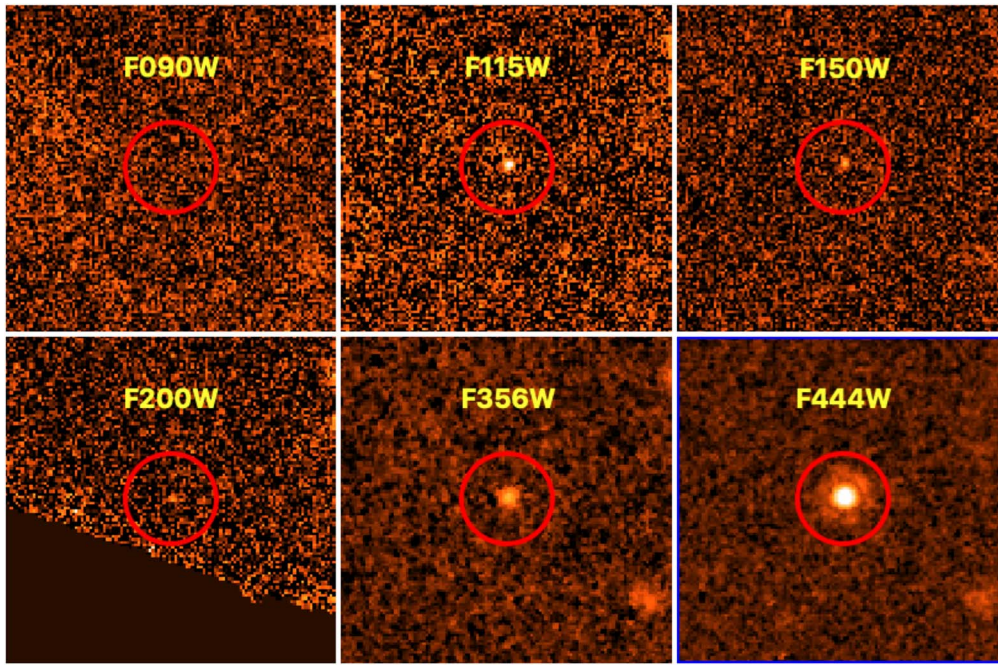
2. Observations

The JWST Director's Discretionary Early Release Science Program ERS 1324 (PI T. Treu; hereafter GLASS-ERS) targets the massive galaxy cluster Abell 2744 with NIRSPEC and NIRISS, and simultaneously images a parallel field 3′–8′ away

---

[*] Based on data collected with JWST.

Figure 1. Image cutouts ($3''5 \times 3''5$) of the GLASS-JWST-BD1 brown dwarf candidate. The circles have a radius of $0''5$. North is up and east is left.

from the cluster with NIRCam in seven broadband filters: F090W, F115W, F150W, F200W, F277W, F356W, and F444W. These observations span the full 1–5 μm range with unprecedented depth and spatial resolution. Details of the GLASS-ERS data acquisition and observing strategy can be found in Treu et al. (2022). Details of the image reduction, stacking, and catalog creation can be found in Merlin et al. (2022).

In the NIRCam parallel data, we visually identified an isolated, very red, and unresolved source, which was particularly bright in F444W. This object immediately appeared to be a potential cool brown dwarf. To search for other cool brown dwarf candidates, we selected from the extracted catalog of Merlin et al. (2022) all sources with CLASS_STAR $\geqslant 0.9$ (point sources), *flags* = 0, F444W $\leqslant 28$ (for reliable photometry in the other bands, see also Castellano et al. 2022), F356W$-$F444 $\geqslant 1.5$, and F115W$-$F444W $\geqslant 2$. The color selection criteria were motivated by the infrared colors of T and Y dwarfs, specifically Spitzer IRAC CH1 $-$CH2 and J$-$CH2 colors (Meisner et al. 2020). Only two sources passed these criteria, with one identified as a diffraction spike from a nearby bright star. We were thus left with the original visually selected candidate, hereafter dubbed GLASS-JWST-BD1 (α, $\delta =$ 00:14:03.33, $-$30:21:21.7). As an isolated source, we can rule out flux contamination from other sources as an explanation for its unusual colors. Figure 1 displays images of the source in six filters, while Table 1 summarizes the relevant photometric data. The source is undetected in F090W. We note that this location is covered by previous Spitzer IRAC CH1 and CH2 observations (Hubble Frontier Fields Program, Lotz et al. 2017), but the object is significantly fainter than the CH2 5σ limit of 24 in those observations (Sun et al. 2021).

3. Analysis

The near- and mid-infrared colors of low-temperature brown dwarfs are greatly affected by molecular absorption bands from

Table 1
Photometric Data for GLASS-JWST-BD1

| Filter	AB	Vega
F090W	$\geqslant 29.0$	$\geqslant 28.5$
F115W	27.766 ± 0.122	27.006
F150W	28.501 ± 0.301	27.301
F200W	29.530 ± 1.345	27.680
F277W	28.789 ± 0.242	26.519
F356W	27.572 ± 0.073	24.812
F444W	25.777 ± 0.011	22.587

Note. Magnitudes have been computed within a $0''56$ diameter aperture. AB to Vega conversion follows Willmer (2018).

H_2, H_2O, CH_4, CO_2, and NH_3 that dominate their spectra (Burrows et al. 2003). The Vega colors of GLASS-JWST-BD1, F115W$-$F444W = 4.55, and F356W$-$F444W = 2.26, are compatible with it being a late-type T dwarf, close to the T/Y boundary (Meisner et al. 2020; Kirkpatrick et al. 2021). To exploit the full photometric information from the NIRCam images, we performed a seven-band spectral energy distribution (SED) fit using JWST/NIRCAM photometry provided with the Sonora Cholla cloudless atmosphere models (Karalidi et al. 2021; Marley et al. 2021).[17] We used the photometric table[18] to compare models and observed photometry in the full model parameter range, 200 K $\lesssim T_{\rm eff} \lesssim$ 2400 K and 3 $\lesssim \log g$ $\lesssim$5.5, provided in the solar metallicity table, with distance moduli spanning 5–15 magnitudes. The best-fit model of $T_{\rm eff} = 700$ K and $\log g = 5.25$ has a reduced $\chi^2 = 6.65$ if we include F277W data. However, if excluding this band, the best-fit model of $T_{\rm eff} = 650$ K and $\log g = 5.25$ has a smaller reduced $\chi^2 = 0.80$ (Figure 2). The flux values of these two best-fit models differ by $<10\%$, and use the $T_{\rm eff} = 650$ K

---

[17] Model: zenodo.org/record/4450269#.Ytqc-S8RrUo.
[18] Photometric table: zenodo.org/record/5063476/files/evolution_and_photometery.tar.gz.
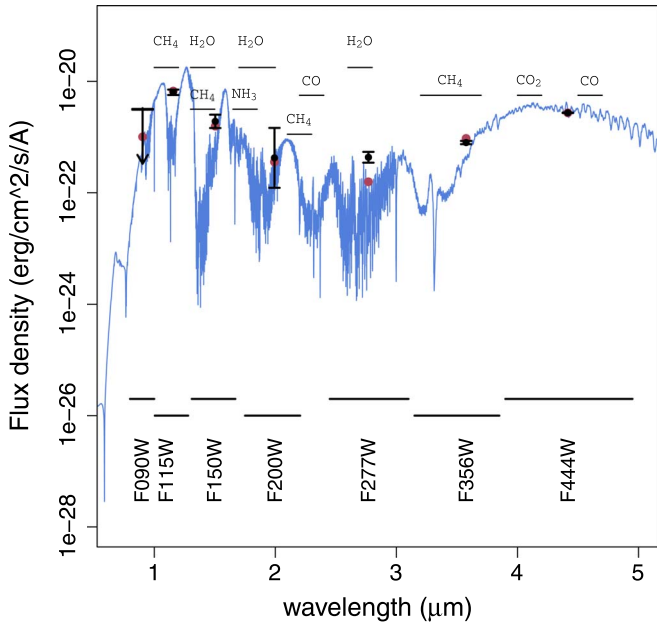
Figure 2. Comparison of observed photometry (black points with 1σ error bars) to the best-fit Sonora Cholla smoothed synthetic spectrum (blue line) and photometry (red points), with $T_{\rm eff} = 650$ K, $\log g = 5.25$, and solar metallicity. We indicate the $> 50\%$ range of the JWST NIRCam filter transmissions used in the GLASS-JWST-ERS observations. Error bars are at 1σ. Note that the source is not detected in the NIRCam F090W filter. Most of the dominant infrared molecular absorption features of H_2O, CO, CO2, CH4, and NH3 are shown.

model for our subsequent analysis. The best scale factor between a model and observed data that depend on the ratio of radius to distance as $\left(\frac{R}{d}\right)^2$ corresponds to a distance modulus of nine (630 pc), assuming $R = 0.83\,R_J$ as provided by the Sonora Cholla models. This temperature corresponds to a spectral type of T8–T9 (Kirkpatrick et al. 2019), consistent with its colors; the temperature and surface gravity together correspond to a mass of $\sim 0.03\,M_\odot$ and an age of ~ 5 Gyr based on the evolutionary models of Marley et al. (2021). GLASS-JWST-BD1 is thus a substellar object. We note that the Sonora Cholla models use equilibrium chemistry, whereas nonequilibrium chemistry is known to play an important role in modulating molecular abundances in T dwarfs, notably CO/CH_4 and NH_3/N_2 (Saumon et al. 2006; Marley & Robinson 2015; Leggett et al. 2021). This may explain the disagreement in F277W photometry, and may also bias our model-inferred physical parameters. We consider these parameters preliminary estimates that may be improved with future modeling.

To determine the absolute magnitude and distance of this source, we used the magnitude/spectral type relations of Kirkpatrick et al. (2021). Here, care needs to be taken with regard to filter systems due to the complex spectral energy distributions of cool brown dwarfs. NIRCAM F444W is a close match to IRAC CH2, and in this band the source is brightest. Using the Sonora Cholla spectra with $T_{\rm eff} = 500$–750 K and $\log g = 3$–5, we find a color offset of $-0.2 \lesssim$ CH2-F444W $\lesssim -0.1$, and adopt a value of -0.15. Applying the absolute CH2/spectral type relation, we estimate absolute F444W magnitudes of 13.65 (T8) and 14.16 (T9), corresponding to distance moduli of 9.30 (T8) and 8.79 (T9), similar to the model scale factor listed above. We therefore infer a distance between 570 pc and 720 pc for GLASS-JWST-BD1, assuming it is a single T8–T9 dwarf.

The total survey volume for T8–T9 dwarfs in the GLASS-ERS NIRCAM parallel field at our F444W = 28 search limit is approximately 7×10^4 pc^3. Kirkpatrick et al. (2021) measured a local space density of $(5.4 \pm 0.6) \times 10^{-3}$ pc^{-3} T8–T9 dwarfs, which would imply up to 370 such sources in the GLASS-ERS NIRCAM parallel field given a uniform spatial density. However, local brown dwarfs are largely members of the Galactic thin disk, and since the Abell 2744 field is close to the South Galactic Pole ($l = 8\overset{\circ}{.}9$, $b = -81°$), we are looking almost vertically out from the Galactic plane. Constraints on the thin disk vertical scale height for brown dwarfs remain uncertain. Ryan et al. (2011) report a scale height of 350 pc for late-M, L, and T dwarfs in a deep HST imaging sample; Aganze et al. (2022) report a scale height of 175 pc—193 pc for T dwarfs with HST parallel spectroscopy. Based on these values, GLASS-JWST-BD1 is ≈ 2–5 scale heights away from the Galactic plane. Adopting a scale height of 300 pc and the local space density from Kirkpatrick et al. (2021), the predicted number of thin disk T8–T9 dwarfs in the Abell 2744 field would be closer to 0.24, which is unlikely, but not unreasonable. Estimates for the space density or distribution of thick disk or halo brown dwarfs remain poorly constrained, but the low number of predicted thin disk late T dwarfs in the Abell 2744 field suggests that GLASS-JWST-BD1 is likely a member of the thick disk or halo population, of which few examples are currently known (Meisner et al. 2020; Schneider et al. 2020).

We investigated other possible explanations for the SED of GLASS-JWST-BD1. The polar direction of this field means that Galactic extinction is negligible, making it highly unlikely that GLASS-JWST-BD1 is a reddened background star; this scenario is also ruled out by its relatively bright F115W magnitude. We also attempted to fit a $z \sim 20$ galaxy model where the Lyman break lies between F356W and F444W. This again cannot explain the emission near 1 μm, which would be completely absorbed by the neutral intergalactic medium; moreover, this solution predicts a much sharper drop between the F356W and F444W filters. We also tried to replicate the SED as a compact galaxy or low-luminosity quasar at $z \sim 8.5$ with extreme [OIII]+Hβ emission in F444W. We fit the photometry to extragalactic templates from the *gsf* code (Morishita et al. 2019). None of the templates using reasonable assumptions of line emission reproduce the observed data points better than the cool brown dwarf model (minimum reduced $\chi^2 = 14.1$).

4. Conclusions

We report the serendipitous discovery of GLASS-JWST-BD1, a faint, distant, and low-temperature brown dwarf. Comparison with theoretical models suggests that the object is a late-type T dwarf with $T_{\rm eff} \approx 650$ K. At its distance, the substellar population is likely dominated by thick disk and halo objects, and GLASS-JWST-BD1 may be such a source. To conclusively demonstrate this, kinematic or chemical abundance data are needed, requiring challenging spectroscopic observations even for JWST. Further information could be gleaned from narrowband imaging or longer-wavelength observations. The large estimated distance of GLASS-JWST-BD1 confirms the power of JWST to probe the very low-mass end of the stellar and substellar mass function in the Galactic thick disk and halo, enabling exploration of metallicity

dependence on low-mass star formation and the evolution of brown dwarf atmospheres.

Facilities: JWST (NIRCam imaging).

Software: gsf (Morishita et al. 2019), SPLAT (Burgasser 2017), ds9 (Smithsonian Astrophysical Observatory 2000), R (R Core Team 2020).

ORCID iDs

Mario Nonino ⬤ https://orcid.org/0000-0001-6342-9662
Karl Glazebrook ⬤ https://orcid.org/0000-0002-3254-9044
Adam J. Burgasser ⬤ https://orcid.org/0000-0002-6523-9536
Gianluca Polenta ⬤ https://orcid.org/0000-0003-4067-9196
Takahiro Morishita ⬤ https://orcid.org/0000-0002-8512-1404
Marius Lepinzan ⬤ https://orcid.org/0000-0003-1287-9801
Marco Castellano ⬤ https://orcid.org/0000-0001-9875-8263
Adriano Fontana ⬤ https://orcid.org/0000-0003-3820-2823
Emiliano Merlin ⬤ https://orcid.org/0000-0001-6870-8900
Diego Paris ⬤ https://orcid.org/0000-0002-7409-8114
Tommaso Treu ⬤ https://orcid.org/0000-0002-8460-0390
Benedetta Vulcani ⬤ https://orcid.org/0000-0003-0980-1499
Xin Wang ⬤ https://orcid.org/0000-0002-9373-3865
Paola Santini ⬤ https://orcid.org/0000-0002-9334-8705
Eros Vanzella ⬤ https://orcid.org/0000-0002-5057-135X
Themiya Nanayakkara ⬤ https://orcid.org/0000-0003-2804-0648
Amata Mercurio ⬤ https://orcid.org/0000-0001-9261-7849
Piero Rosati ⬤ https://orcid.org/0000-0002-6813-0632
Claudio Grillo ⬤ https://orcid.org/0000-0002-5926-7143
Marusa Bradac ⬤ https://orcid.org/0000-0001-5984-0395

References

Aganze, C., Burgasser, A. J., Malkan, M., et al. 2022, ApJ, 924, 114
Burgasser, A. J. & Splat Development Team 2017, in ASI Conf. Ser. 14, Proc. of the Int. Workshop on Stellar Spectral Libraries (IWSSL 2017), ed. P. Coelho, L. Martins, & E. Griffin (ASI: Hyderabad), 7
Burgasser, A. J., Kirkpatrick, J. D., Burrows, A., et al. 2003, ApJ, 592, 1186
Burrows, A., Sudarsky, D., & Lunine, J. I. 2003, ApJ, 596, 587
Castellano, M., Fontana, A., Treu, T., et al. 2022, ApJL, 938, L15
Chabrier, G., & Baraffe, I. 2000, ARA&A, 38, 337
Karalidi, T., Marley, M., Fortney, J. J., et al. 2021, ApJ, 923, 269
Kirkpatrick, J. D. 2005, ARA&A, 43, 195
Kirkpatrick, J. D., Gelino, C. R., Faherty, J. K., et al. 2021, ApJS, 253, 7
Kumar, S. S. 1962, AJ, 67, 579
Kirkpatrick, J. D., Martin, E. C., Smart, R. L., et al. 2019, ApJS, 240, 19
Leggett, S. K., Tremblin, P., Phillips, M. W., et al. 2021, ApJ, 918, 11
Lotz, J. M., Koekemoer, A., Coe, D., et al. 2017, ApJ, 837, 97
Marley, M., & Robinson, T. 2015, ARA&A, 53, 279
Marley, M. S., Saumon, D., Visscher, C., et al. 2021, ApJ, 920, 85
Masters, D., McCarthy, P., Burgasser, A. J., et al. 2012, ApJL, 752, L14
Meisner, A. M., Faherty, J. K., Kirkpatrick, J. D., et al. 2020, ApJ, 899, 123
Merlin, E., Bonchi, A., Paris, D., et al. 2022, ApJL, 938, L14
Morishita, T., Abramson, L. E., Treu, T., et al. 2019, ApJ, 877, 141
R Core Team 2020, R: A Language and Environment for Statistical Computing, R Foundation for Statistical Computing, Vienna, Austria, https://www.R-project.org/
Ryan, R. E., Thorman, P. A., Yan, H., et al. 2011, ApJ, 739, 83
Saumon, D., Marley, M. S., Cushing, M. C., et al. 2006, ApJ, 647, 552
Schneider, A. C., Burgasser, A. J., Gerasimov, R., et al. 2020, ApJ, 898, 77
Smithsonian Astrophysical Observatory 2000, SAOImage DS9: A utility for displaying astronomical images in the X11 window environment, Astrophysics Source Code Library, ascl:0003.002
Sun, F., Egami, E., Pérez-González, P. G., et al. 2021, ApJ, 922, 114
Treu, T., Roberts-Borsani, G., Bradac, M., et al. 2022, ApJ, 935, 110
Willmer, C. N. A. 2018, ApJS, 236, 47
Zhang, Z. H., Burgasser, A. J., Gálvez-Ortiz, M. C., et al. 2019, MNRAS, 486, 1260